A Simple Method for Estimating Monthly Mean Albedo of Land Surfaces From AVHRR Data

GEORGE GUTMAN

Cooperative Institute for Climate Studies, University of Maryland, College Park, Maryland

(Manuscript received 6 August 1987, in final form 13 January 1988)

ABSTRACT

It is suggested that the observed periodicity of cloud-free, visible and near-infrared data from the Advanced Very High Resolution Radiometer (AVHRR) onboard NOAA-9 for a particular target can be efficiently used for deriving the monthly mean clear-sky planetary albedo. The broadband albedo is approximated by a linear combination of visible and near-infrared albedos. The new method of 9-day compositing distributes the clear-sky observations over the sun-target-sensor geometry combinations and weights them by the occurrence of each combination during a particular month. It is shown that the monthly mean clear-sky planetary albedo can be estimated solely from the visible and near-infrared data in a model-independent manner. The surface albedo is then obtained by applying a simple atmospheric correction to the derived clear-sky planetary albedo.

A comparison of the results of the present method and those obtained by using the "minimum albedo" method indicates that the latter may lead to an underestimation of monthly values because of the angular variation in clear-sky observed albedos. The derived surface albedos are compared with those reported in climatological studies based on ground observations.

1. Introduction

Satellite measurements of clear-sky radiances are affected by the various combinations of sun-target-sensor geometry, and by atmospheric scattering and absorption. The latter factors, in turn, vary with wavelength. The complexity of the general problem in quantification of surface characteristics was outlined in a comprehensive review by Duggin (1985). Derivation of the clear-sky surface albedo from satellite data is further complicated by the limited number of clear views, by limited sampling of the complete sun-target-sensor geometry, and by the time variation of the atmospheric constituents and surface properties. Reviews of the scientific studies aimed at inferring planetary and surface clear-sky albedos from satellite information can be found in Pinker (1985) and in Matthews and Rossow (1987). There have been some extensive studies using data from GOES (Minnis and Harrison 1984; Briegleb et al. 1986) as well as from METEOSAT (Pinty and Szejwach 1985; Dedieu et al. 1987). Not much has been done, however, with data obtained from the polar-orbiting NOAA satellites. The few studies on determination of albedo have used the so-called "minimum albedo" method (e.g. Geleyn and Pruess 1983). This approach is based on the assumption that the minimum of observed albedos during a certain period of time would best represent the clear-sky planetary albedo. It works fairly well for an isotropic system, but fails, as is demonstrated in the present study, in the case of the earth-atmosphere system.

The NOAA-9 Advanced Very High Resolution Radiometer (AVHRR) data counts (proportional to the observed radiances) are presently converted into albedo units using a linear regression relationship (see e.g. Rao 1987) so that the reflectance factor in such datasets can be represented by:

$$r_i = \pi L_i / S_i \quad (i = 1, 2) \tag{1}$$

where L_i is the filtered radiance detected by the satellite sensor, S_i the filtered solar irradiance at normal incidence at the mean earth-sun distance, and i denotes the AVHRR channels 1 and 2. On the other hand, the albedo A_i is generally defined as a ratio of the reflected irradiance F_i to the solar irradiance S'_i incident onto a horizontal plane for a specific earth-sun distance:

$$A_i = F_i / S'_i \mu \tag{2}$$

where μ is the cosine of the solar zenith angle. From (1) and (2), we have:

$$A_i = F_i r_i / \pi L_i \mu f, \tag{3}$$

where $f = S'_i / S_i$ is a correction factor accounting for variation in the earth-sun distance. Its contribution of about 3% in the annual variability of albedo is neglected here in comparison with the observed albedo variability discussed below.

Corresponding author address: Dr. George Gutman, NOAA/NESDIS/LSB-E/RA12, Room 712, World Weather Building, Washington, DC 20233.

Assuming that the radiation field is isotropic and that its intensity is equal to L_i, the effective isotropic albedo of channel i can be presented by

$$\alpha_i = r_i/\mu \tag{4}$$

and will be referred to hereafter as observed albedo.[1] Thus, if the earth-atmosphere system were isotropic, the changes in albedo observed at the same solar time in clear-sky conditions would be caused in large part, by the time variation in the atmospheric and surface properties. It is known, however, that the above assumption of isotropy is invalid for the earth-atmosphere system. The anisotropic properties of this system have been studied, for example, by Taylor and Stowe (1984a) and by Koepke and Kriebel (1987). It has also been shown that variation in observed clear-sky albedos for a particular target derived from mapped AVHRR data is periodic and induced by the systematic variation in sun-target-sensor geometry (Gutman 1987). The period of variation (9 days) in recorded data can be explained as follows. The nodal period of the NOAA-9 satellite (time between two consecutive equator crossings in the ascending node) is equal to 102 min., which means slightly more than 14 orbits each 24 h. Figure 1 shows the N^{th} orbit and the $(N + 14)^{th}$ orbit the next day. The shift between these two orbits is 2.74° (CD in Fig. 1). As the orbital swath (BD) is equal to 25.5°, it takes about 9 days for the N^{th} orbit to "get into phase" so that point D reaches point B. In other words, the geometry of the N^{th} orbit will be repeated *almost* exactly by the $(N + 127)^{th}$ orbit. The 9-day oscillation of the solar zenith angle is modulated by a lower frequency seasonal oscillation (Fig. 2).

The anisotropic factor can be defined by

$$\Omega_i(\phi, \Theta, \Theta_s) = \pi L_i/F_i, \tag{5}$$

where ϕ is the relative azimuth (difference between the solar and satellite azimuths), and Θ and Θ_s are satellite and solar zenith angles, respectively. Combination of (3)–(5) yields a relationship between the *observed* and the *true* channel i albedos:

$$A_i = \alpha_i/\Omega_i(\phi, \Theta, \Theta_s). \tag{6}$$

This implies that in order to infer the midafternoon (NOAA-9 day-time pass) true channel i albedo from the instantaneous clear-sky observations, the anisotropic factor must be known as a function of surface type and sun-target-sensor geometry for each channel. To our knowledge, however, narrow-band vegetation type dependent tables of anisotropic factors (or bidirectional models) have not yet been constructed.

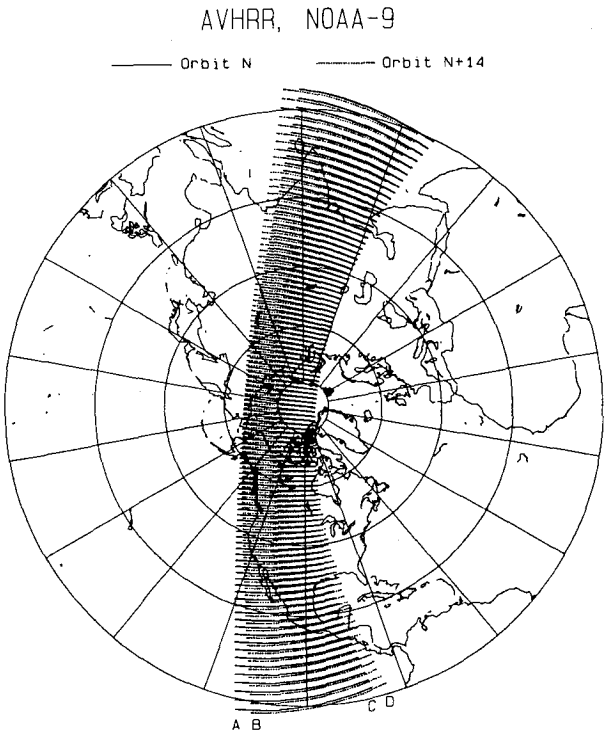

FIG. 1. Scan patterns of the AVHRR onboard NOAA-9 for two consecutive days: N^{th} and $(N + 14)^{th}$ orbits.

Koepke and Kriebel (1987) noticed that the anisotropic factors derived from large-scale data must be used cautiously in higher resolution datasets and recommended deriving them separately for each of the surface types using "very realistic model assumptions." Furthermore, if one decides to use an existing broadband "average land" model (e.g. Taylor and Stowe 1984a), the necessary information (ephemeri data used for calculating ϕ, Θ, and Θ_s) is not always included in the da-

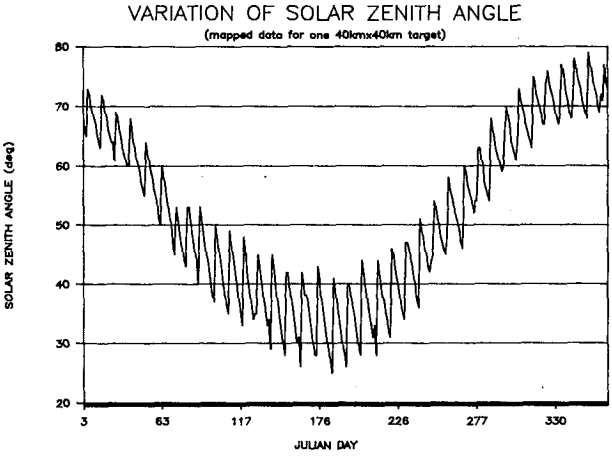

FIG. 2. Variation of solar zenith angle (mapped data over a 40-km by 40-km target during 1986).

[1] In satellite literature, the terms visible (near-infrared) albedo, reflectance and scaled radiance are used interchangeably. The term "observed albedo" is preferred here to emphasize the difference between the "observed" and "true" albedos, which would be equal in the case of the isotropic system.

tasets and/or may not be readily available on magnetic tapes. In this case, determination of the true albedo on a daily basis seems infeasible.

One of the problems that can be addressed in the absence of a bidirectional model is the determination of a mean clear-sky albedo for a certain period of time defined as:

$$\langle A \rangle = \langle \alpha\mu \rangle / \langle \mu \rangle, \tag{7}$$

where $\langle\ \rangle$ denotes a time average and α is the broadband albedo inferred from the observed channel 1 and 2 albedos. To solve such a problem, one should consider a period of time (not shorter than 9 days), that would contain a sufficient number of clear-sky observations to comprise the complete cycle of sun-target-sensor geometry.

In the ideal case, when the whole period is clear sky, one would be able to estimate mean values for 9 days, 18 days, etc. Usually, however, a large portion of the data is rejected as cloud-contaminated. Therefore, there is no guarantee that all sun-target-sensor geometry combinations for clear-sky data will be equally represented in a straightforward averaging procedure described by (7): i.e., inadequate sampling may lead to errors in albedo estimates.

The present study suggests a method of determining the mean planetary albedo by weighting the observations proportional to the frequency of occurrence of the corresponding sun-target-sensor geometry combinations during the period of interest. Derivation of monthly mean clear-sky planetary albedo is model-independent since it is reduced to mere reprocessing the visible and near-infrared AVHRR data. The ultimate goal—estimation of monthly mean surface albedo—is reached by applying a narrow to broadband conversion and a simple atmospheric correction.

2. Satellite data

Data for this study were extracted from a dataset collected over the United States Great Plains by NOAA/NESDIS. Daily AVHRR GAC data from NOAA-9 were mapped to a polar stereographic projection with a resolution of 10 km so that the final map represented a 10 km sample of 4-km by 1-km GAC pixels. The daily 10-km resolution maps were averaged over 16 values of 4 by 4 arrays of the 10-km cells. The reduced resolution data were mapped to a 40-km polar stereographic projection. Description of this dataset is given in greater detail in Gallo et al. (1984) and Gutman et al. (1987).

The data used consist of means and standard deviations of the 40-km by 40-km map cells. Four such cells were chosen to represent four vegetation types: 1) shrub savanna in southwestern Texas (30°N, 101.7°W); 2) mixed forest in northwestern Minnesota (47.3°N, 95.6°W); 3) grama-buffalo grass in southwestern Oklahoma (34.5°N, 98.7°W); and 4) bluestem prairie in central Kansas (38.9°N, 98°W).

These four targets (vegetation types) will be hereafter referred to as desert, forest, grass and prairie, respectively. The choice of these target areas was governed by an apparent (from a Landsat photograph) homogeneity of terrain, by the difference in vegetation type and by the frequent occurrence of the clear-sky views.

3. Methodology

Derivation of total albedo from spectral albedos involves narrow-to-broadband conversion. This has been discussed, for example, by Pinker and Ewing (1986). The present study employs a linear relationship for vegetated surfaces suggested by Wydick et al. (1987), wherein the regression statistics for different surface types were derived from angularly-matched ERB broadband and AVHRR narrowband bidirectional reflectances. The observed broadband albedo is approximated by

$$\alpha = -0.70 + 0.36\alpha_1 + 0.73\alpha_2, \tag{8}$$

where subscripts "1" and "2" denote visible and near-infrared observed albedos, respectively. Those are calculated from (4) using AVHRR channel 1 and 2 data.

The data for the analysis are first "cloud screened" using a technique described in Gutman et al. (1987). The cloud screening involves a combination of three masks: thermal and visible gross filters and a spatial coherence visible fine filter. For this study, the surface temperatures calculated by the split-window technique were restricted to be higher than the monthly minimum of the midafternoon air temperature at shelter level. The α was restricted to values lower than 40% and the standard deviations of visible reflectances were not allowed to exceed the monthly minimum value by more than 0.5% albedo units.

Figure 3 shows the variation of α for the four target areas during July 1986. A sufficient number of clear-sky views allows us to trace the systematic behavior of α in all four targets, indicative of the adequacy of the cloud-screening.

How can these data be efficiently used for obtaining a monthly mean estimate? The "minimum albedo" method (Ellis and Vonder Haar 1978) will obviously lead to an underestimated value due to the large range of variation in the observed albedos. Averaging as in (7) may be inadequate due to the sampling problem discussed earlier. One could attempt averaging a periodic function that approximates the scattered data. However, some weeks do not contain sufficient data points to construct such a Fourier-type function.

It is proposed that one make use of the periodicity and superimpose all data for each month on a 9-day cyclic interval. This procedure (hereafter referred to as "compositing") consists of splitting each month of cloud-free data into 9-day periods and superimposing

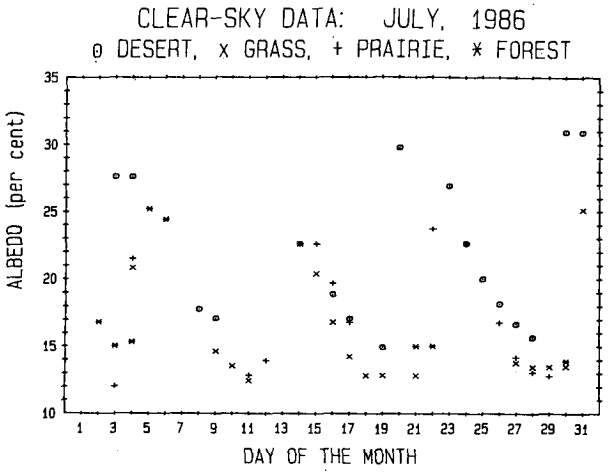

FIG. 3. Clear-sky broadband albedo inferred from observed visible and near-infrared albedos for four targets during July 1986.

the corresponding days from each period. For display purposes, the composited observations are sorted so that the maximum of the solar zenith angle occurs on the first day of compositing. The result of such a procedure is shown in Fig. 4. The monthly mean value can then be derived in two further steps: (i) the original cloud-free data for each day of compositing are averaged, and (ii) the averages for each day of compositing are averaged over the 9-day compositing interval.

This method essentially distributes the data over the various sun-target-sensor geometry combinations, i.e., three-dimensional angular bins (ϕ, Θ, Θ_s), without actually employing the angular information but making use of the periodicity in the observed albedo as related to the variation in sun-target-sensor geometry. The anisotropy of the system is accounted for indirectly without using a bidirectional model. Taylor and Stowe (1984b) showed that the anisotropic patterns of the land reflectance in the azimuthal plane are asymmetric. The present method will work better when data are obtained from scanning in the principal plane (the relative azimuth is 0° or 180°) or close to it, since in this case there is greater probability that collected data will represent most of the anisotropic variability in albedo. The deviation of the scanning direction from the principal plane depends upon latitude and season. For midlatitudes, the cross-track scanner of the NOAA-9 AVHRR scans close to the principal plane during the period between spring and autumn. It can be tentatively concluded that the present method will be more reliable in its application to data collected over the areas in temperate latitudes during the growing season, but may be less accurate when the solar zenith angle is large, i.e., in high latitudes and/or during the fall–winter period.

Thus, it is suggested to calculate the monthly mean clear-sky planetary albedo from

$$\langle A \rangle = \{\bar{\alpha}\bar{\mu}\}/\{\bar{\mu}\}, \tag{9}$$

where $\langle\ \rangle$ and $\{\ \}$ denote clear-sky monthly mean and 9-day full cycle mean, respectively, and the overbar denotes averaging on each day of compositing. It should be noted that the viewing geometry of the AVHRR scanner is limited to 50° off nadir. Therefore, averaging over the compositing interval, which covers only a portion of the whole hemisphere, may introduce some error in the approximation of the mean hemispheric albedo.

Note that $\langle A \rangle$ represents the mean value of albedo at midafternoon. Briegleb and Ramanthan (1982) showed that the diurnal average planetary albedo is very close to the albedos observed around 0900 LST and 1500 LST. The day-time pass of NOAA-9 is between 1400 LST and 1500 LST. Therefore $\langle A \rangle$ can be regarded as an approximation of the monthly mean of diurnal average clear-sky planetary albedo. This will hold well during the first two or three years from the satellite launch. However, the orbit degradation during the consequent years leads to a later observation time (i.e., greater solar zenith angle) which will result in greater error of the derived albedo. One could derive monthly mean albedo from the integral of the albedo as a function of the solar zenith angle using an existing directional model (e.g., Taylor and Stowe 1984a,b). However, such an approach will make the present method model dependent and therefore is not used here.

In order to derive the surface albedo from the planetary albedo, the latter should be corrected for the atmospheric effects. This is usually accomplished by applying radiative transfer models. The present study makes use of a simple method proposed by Chen and Ohring (1984), which suggests a linear relationship between clear-sky planetary and surface albedos for an aerosol free atmosphere. Results of Chen and Ohring (1984) correlate well with those obtained with an independent model (Pinker 1987, personal communication) and are consistent with the results of Koepke

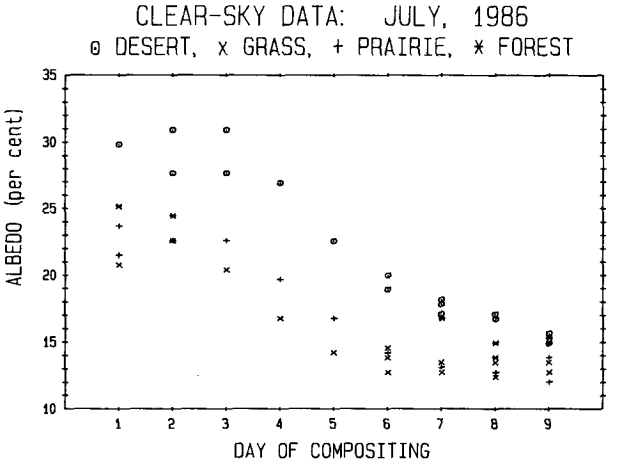

FIG. 4. Same as in Fig. 3 composited over the 9-day interval.

and Kriebel (1987). Following Chen and Ohring, the monthly mean surface albedo is estimated by

$$\langle A_s \rangle = a + b\langle A \rangle, \tag{10}$$

where a and b are coefficients dependent upon solar zenith angle. Note that Chen and Ohring (1984) obtained the regression of A on A_s. Since the coefficients a and b were derived directly from the original Chen and Ohring formula, they may differ slightly from those which would be obtained from the regression of A_s on A. Strictly speaking, the surface albedo is a function of cloudiness. However, the diffuse component in the surface albedos for vegetated surfaces can be neglected (Hummel and Reck 1979). Therefore, the derived clear-sky surface albedo will accurately represent the average surface albedo.

4. Data analysis and results

As discussed earlier, the angular variation of the observed albedo depends upon a *combination* of three angles: solar zenith, satellite zenith (or nadir) and relative azimuth, representing the sun-target-sensor geometry. Neither azimuth nor any indication of the scanning direction (forward or backward) were archived in this dataset. In this situation the compositing procedure has proven to be very useful: the scanning direction was restored assuming that its change occurred around the fifth day of each 9-day period. Forward scanning direction (towards the sun) is defined as positive. Figure 5 illustrates the close relationship between solar zenith and satellite off-nadir viewing angles for the AVHRR observations over one target during July 1986. It can be concluded that discrimination between the solar zenith and satellite viewing angle effects is difficult in AVHRR data. However, it follows from previous studies (Taylor and Stowe 1984a,b) that in a narrow range of solar angles, the variation in reflectivity is mainly due to changes in the relative azimuth from back- to forward scanning direction.

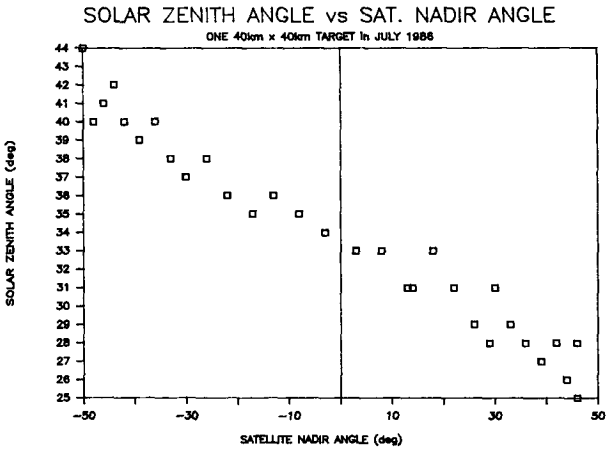

FIG. 5. Relationship between solar zenith angle and satellite nadir angle for one target during July 1986.

It has been demonstrated that the variation of α within the 9-day period is quite systematic for each vegetation type under consideration. It should be noted herein that the duration of a monotonic progression of mapped data may not always be 9 days but may vary from 8 to 10 days. This is a result of the mapping from overlapped orbits. In such cases, the outliers at the first or last days of compositing should be reassigned respectively to the end or beginning of the interval. The wide range of variation of observations within the interval facilitates this task. In the present study, the reassignment was done if the current value was greater (at the last day) or less (at the first day) than the mean over the interval. Note also that if sun-target-sensor geometry repeated itself exactly, then for each day of the compositing interval, α would also repeat itself exactly, with all else being equal. However, because of a slight difference between the angular combinations on the corresponding days from the 9-day periods of a given month and due to natural changes in the atmosphere and at the surface, the values of α are somewhat scattered on each day of the compositing interval (see Fig. 4). Further analysis is performed on composited distributions of α averaged for each day of compositing using (7) and denoted by $\bar{\alpha}$.

Arrays of $\bar{\alpha}$ (month, day of compositing) for each target were objectively analyzed using the interpolation scheme of Thomasell (1979). Missing observations were filled in and the fields of $\bar{\alpha}$ were smoothed to allow for the uncertainties caused by an insufficient number of observations on some days of compositing. Several months of data from the previous (1985) and subsequent (1987) years were used to improve the performance of the interpolation scheme at the boundaries. Figures 6, 7, 8 and 9 show $\bar{\alpha}$ as a function of the day of compositing for different months of 1986.

The common feature of virtually all of the curves is monotonic decrease from the first to the last day of the compositing interval (i.e., from extreme backscattering to extreme forward scattering). In some instances, however, the curve rises slightly at the end of the compositing interval. This is a manifestation of the increase in bidirectional reflectance for high values of satellite viewing angles in the forward scanning direction when the solar zenith angle becomes large (Taylor and Stowe 1984b). This effect occurs mostly during the period of the rapid increase in the solar zenith angle between the autumnal equinox and the winter solstice.

Monthly mean planetary albedo was calculated from (9) by piecewise numerical integration (using the trapezoid rule): $\{\bar{\alpha}\bar{\mu}\} = (\sum (\bar{\alpha}\bar{\mu})_i/8) - ([(\bar{\alpha}\bar{\mu})_1 + (\bar{\alpha}\bar{\mu})_9]/16), \{\bar{\mu}\} = (\sum \bar{\mu}_i/8) - ((\bar{\mu}_1 + \bar{\mu}_9)/16)$, where $\sum$ denotes summation overall compositing days ($i = 1$–9). A comparison of these results with those obtained by applying the minimum-albedo method and those obtained by averaging all monthly clear-sky ob-

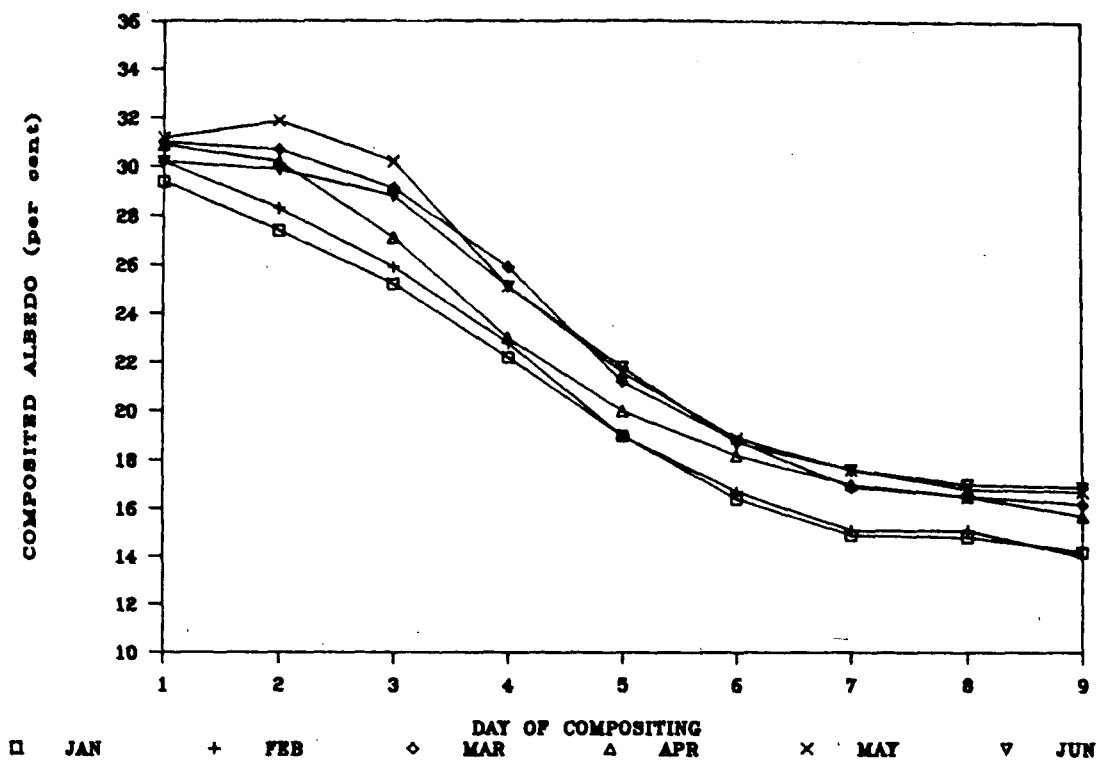

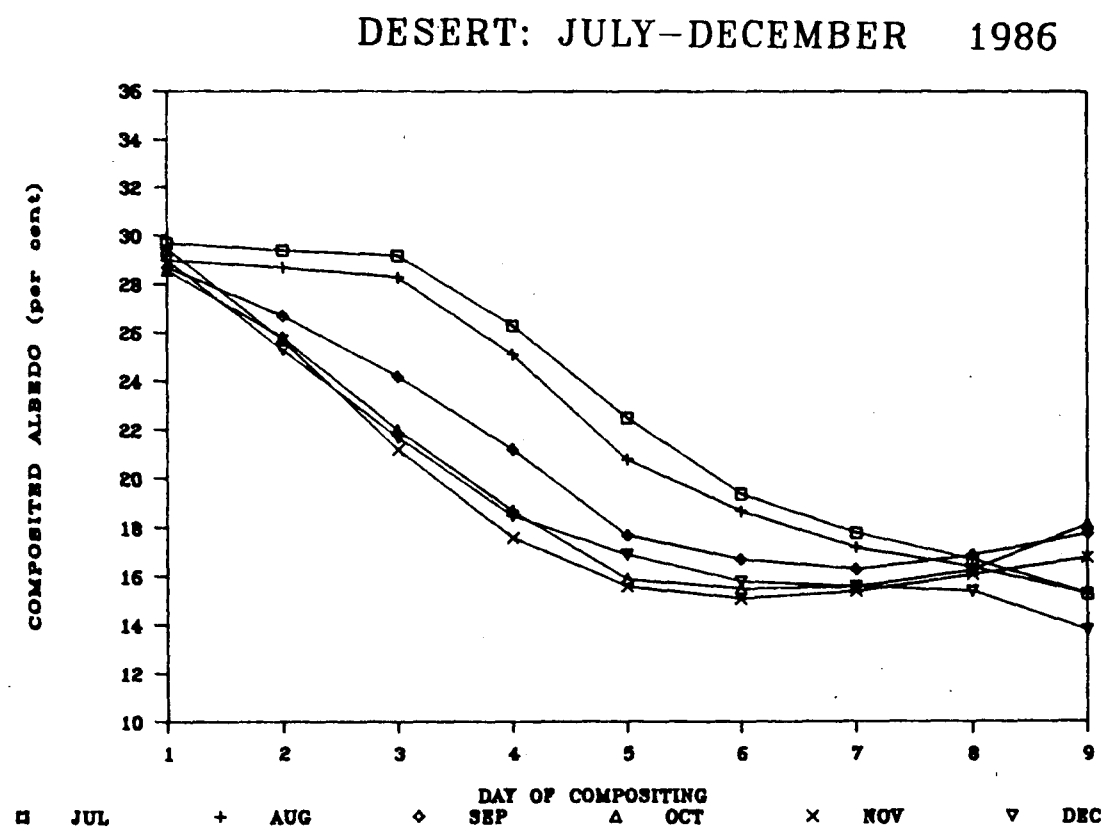

FIG. 6. Monthly distribution of the composited albedo over the 9-day interval: desert. Top: January (□), February (+), March (◇), April (△), May (×), June (▽). Bottom: July (□), August (+), September (◇), October (△), November (×), December (▽).

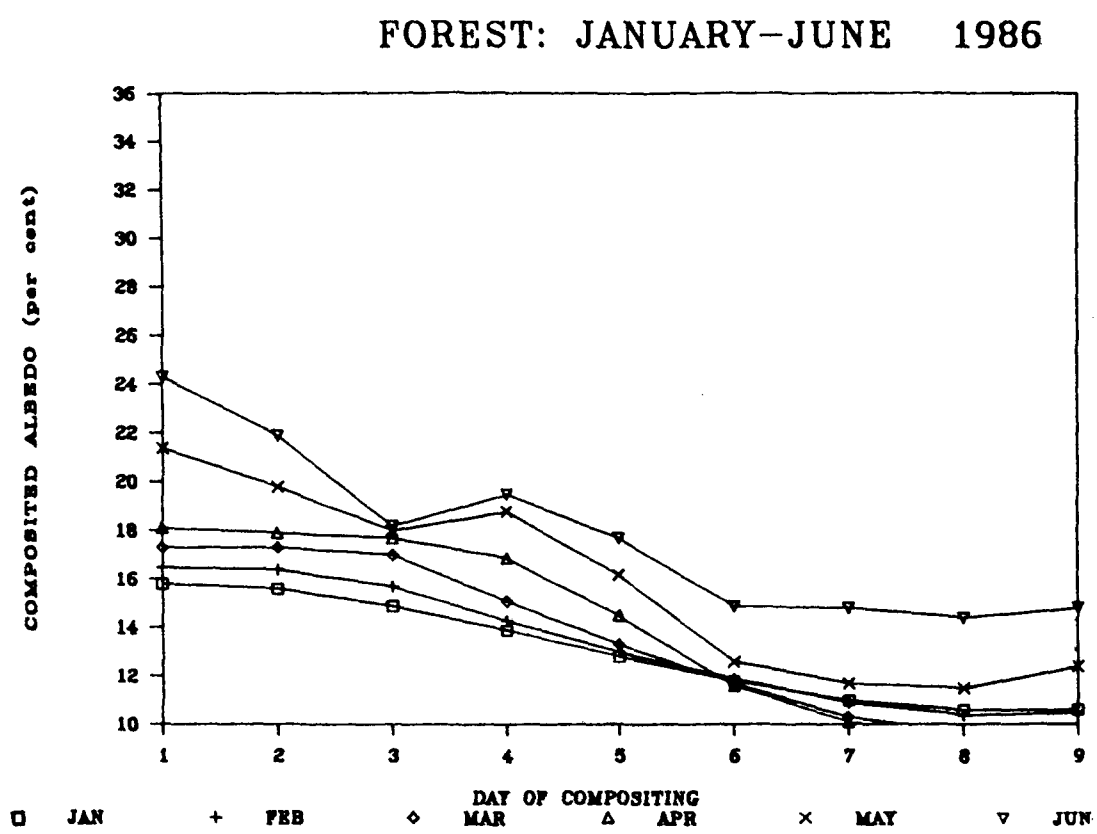

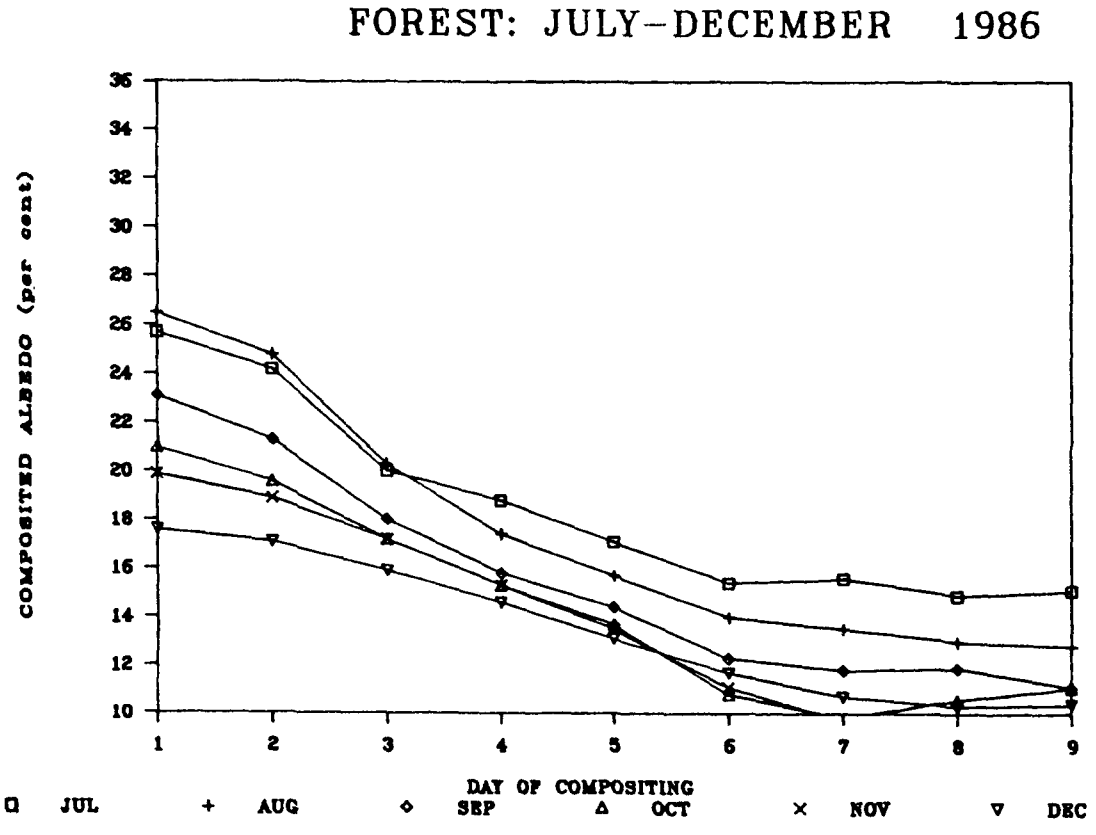

FIG. 7. Same as in Fig. 6 for forest.

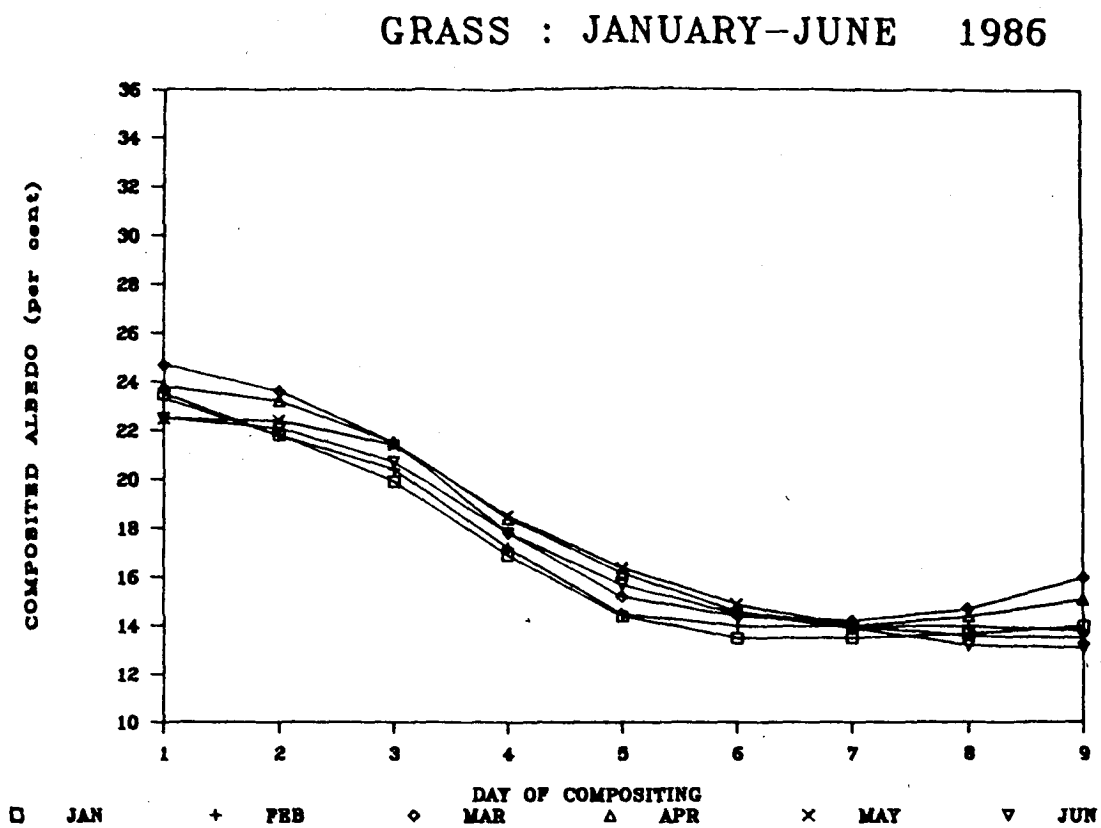

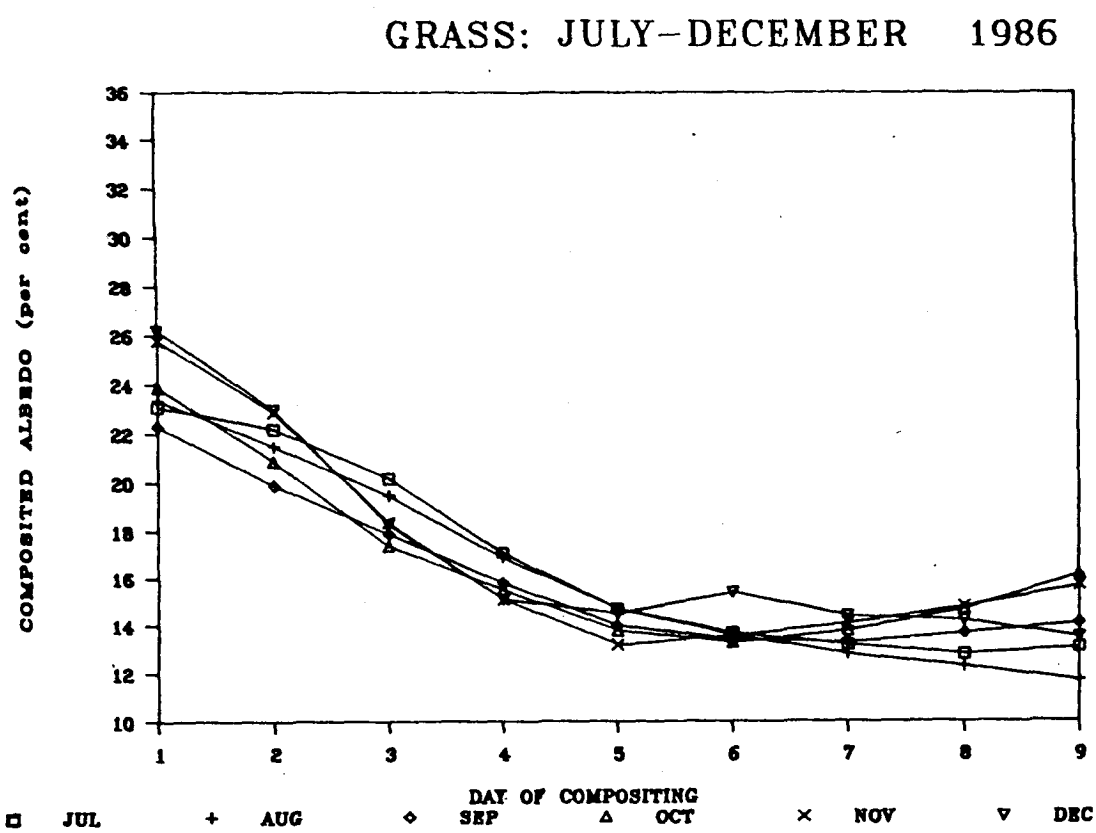

FIG. 8. Same as in Fig. 6 for grass.

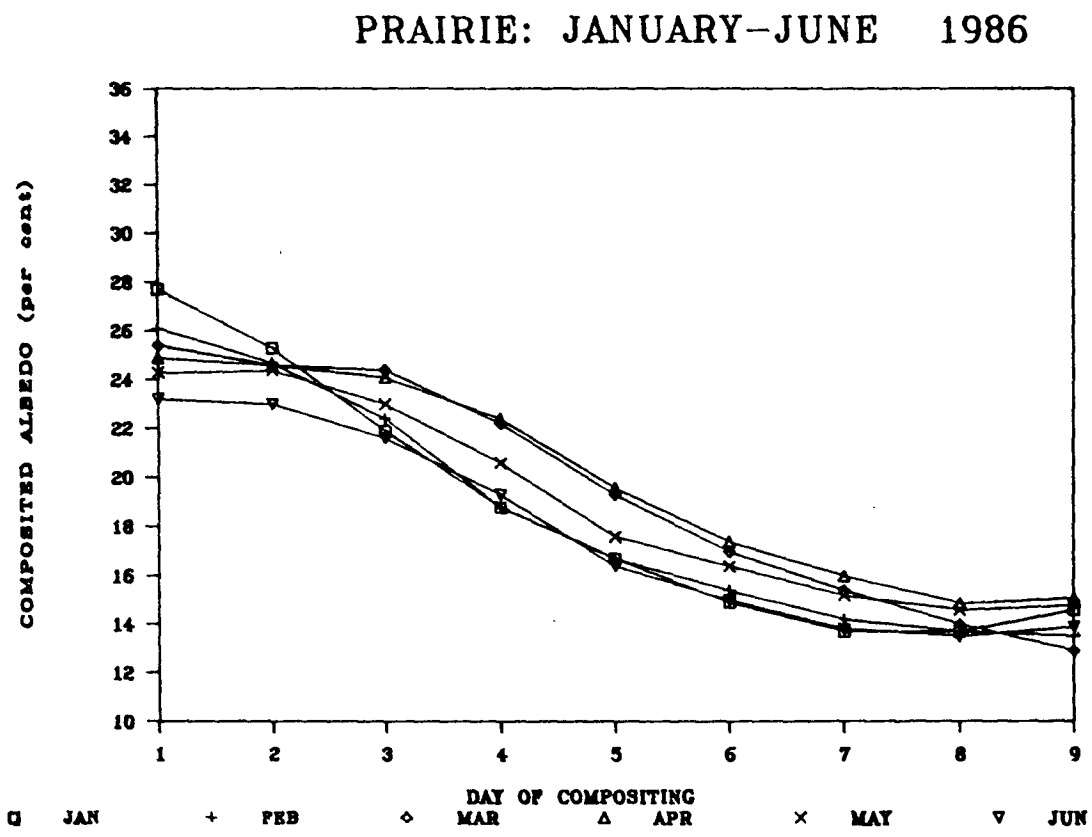

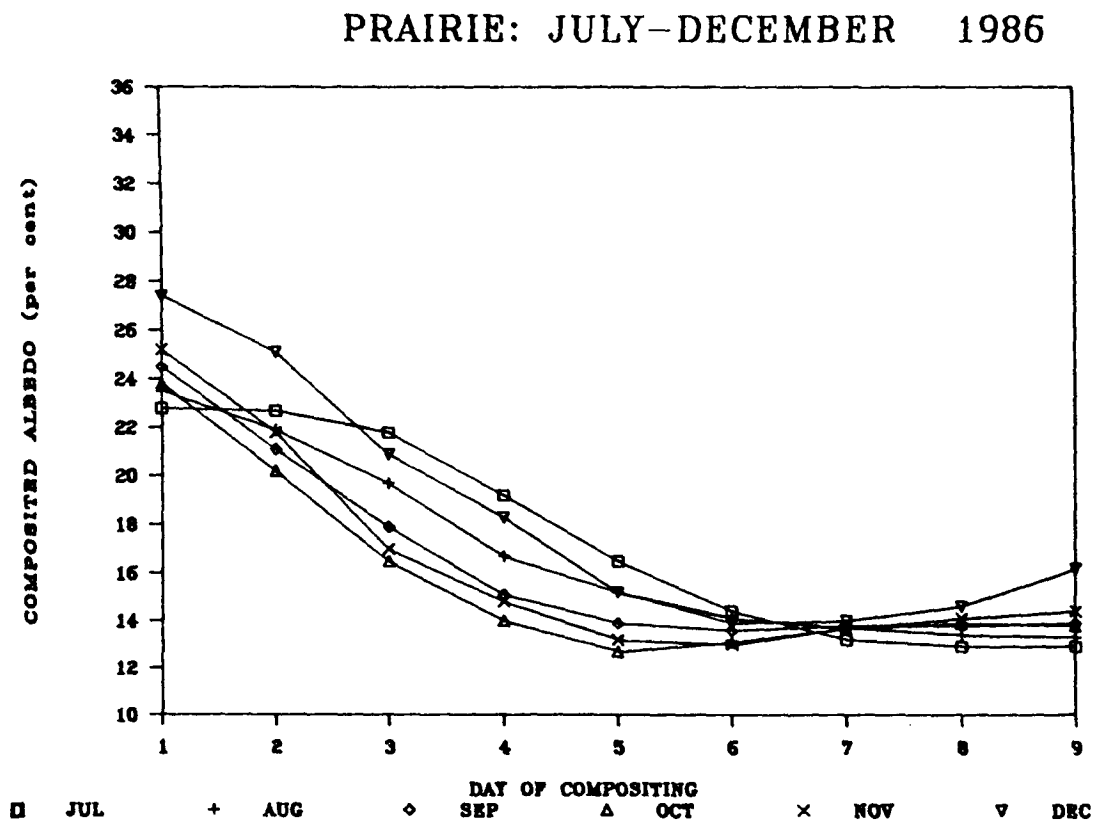

FIG. 9. Same as in Fig. 6 for prairie.

servations equally weighted ("simple averaging") is given in Figs. 10 and 11.

The problems associated with considering the minimum value as a "true planetary clear-sky albedo" have been discussed previously by Pinker and Razgaitis (1983) and by Matthews and Rossow (1987). Figures 10 and 11 demonstrate that such an approach may underestimate monthly clear-sky planetary albedo by as much as 40% relative to the mean. They also show that the difference of the means obtained by two methods (compositing versus simple averaging) can be relatively large. This difference depends upon sampling, i.e., the distribution of observations over sun-target-sensor geometry. Sometimes simple averaging may yield the required accuracy. Without compositing, however, there is no control over the distribution of observations with respect to the geometry combinations. Perhaps all of the available observations will group in the beginning or end of the compositing interval, and then simple averaging will lead to erroneous results. In our example, during particular months observations are more or less evenly distributed over the 9-day compositing interval (due to the choice of the target areas), which results in small differences between the two calculated means for those months.

Actually, the method of compositing can also be regarded as a tool for making a decision as to whether the available data can or cannot be efficiently used for estimating the mean albedo. On the other hand, the advantage of the suggested approach is that it allows missing data to be filled in because of the revealed functional behavior of $\bar{\alpha}$ with respect to a day of compositing.

One of the validation tests of the present method could be a comparison of the derived monthly mean clear-sky planetary albedos with those that would result from monthly averaging of daily observed albedos corrected using a bidirectional model. Preliminary results on applying the broadband "average vegetated land" bidirectional model of Taylor and Stowe (1984a) to these data are encouraging (Gruber et al. 1987). The values obtained by averaging the corrected albedos for the month of July are shown (by an asterisk) in Figs. 10 and 11. It should be noted, however, that such a comparison would not be conclusive since the results would be model-dependent. As mentioned earlier, bidirectional models are to be site specific and based on high resolution data (Koepke and Kriebel 1987).

Finally, the monthly mean surface albedos A_s were calculated from (10). Their monthly distributions for

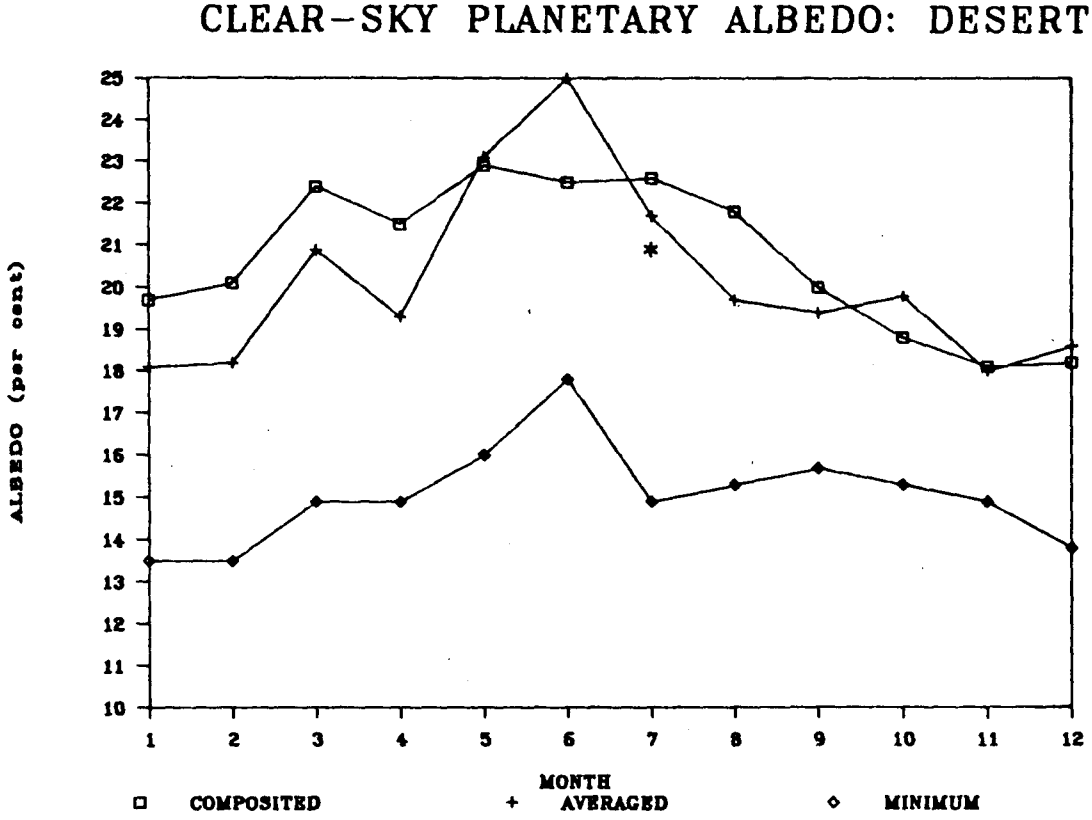

FIG. 10. Annual variation of monthly mean clear-sky planetary albedo obtained by the present method (composited), by simple averaging irrespective of sun-target-sensor geometry (averaged), and by taking minimum albedo (minimum) for each month. Desert (top) and forest (bottom). Asterisk indicates the value obtained for July by averaging over the albedos corrected with a bidirectional model.

the four vegetation types are shown in Figs. 12 and 13. The derived albedos are compared with those reported by Matthews (1985) and by Hummel and Reck (1979). In these studies, the ground observations on albedo of various surface types over the globe were compiled from different sources. The albedo values were extracted from Matthews' 1° by 1° resolution map. The desert and the forest targets are situated between the boxes of different vegetation types of Matthews' classification. Therefore, two vegetation types located close to our targets are shown in Fig. 12 for both desert and forest. The vegetation types used for comparison, and their symbols in Matthews' classification are: drought-deciduous shrubland/thicket (19), xeromorphic shrubland/dwarf shrubland (21), temperate/subpolar evergreen needle leaved forest (8), cold-deciduous forest without evergreens (11), meadow/short grassland (28), and medium grassland (27). The values for all of the months were found by interpolating between those of January, April, July and October reported in Matthews (1985). From Hummel and Reck (1979), four surface types were taken for comparison: desert/shrubland (1), mixed coniferous and deciduous forests (2), arable land with intensive farming (3), and grazing and marginal farming lands (4). Although the 40 km × 40 km targets are relatively homogeneous, they definitely contain more than one vegetation type as well as bare soil. Thus, the derived albedo represents an average value for a mixture of different surface types. This should be noted when comparing satellite-derived albedo with that of a specific vegetation type based on ground observations.

The annual variations of the derived albedos for all four vegetation types agree fairly well with those given by Matthews (1985) and Hummel and Reck (1979). The amplitude of the annual variation of the surface albedos is greater than that of the corresponding planetary albedos. This is due to the dependence of the atmospheric correction on the solar zenith angle. The derived albedos lie between the values of the corresponding types reported by the above authors for the most part of the year. In the autumn months, the present results seem to underestimate the surface albedos. It might partially be a result of the present method's deficiency when solar zenith angles become large. It could also be due to the AVHRR degradation during the fall of 1986 (Jacobowitz et al. 1987).

5. Summary and conclusions

It has been demonstrated that AVHRR data can be used efficiently for estimating monthly mean surface albedo. The procedure consists of the following steps:

1) Reorganization of the data by 9-day satellite repeat cycle.

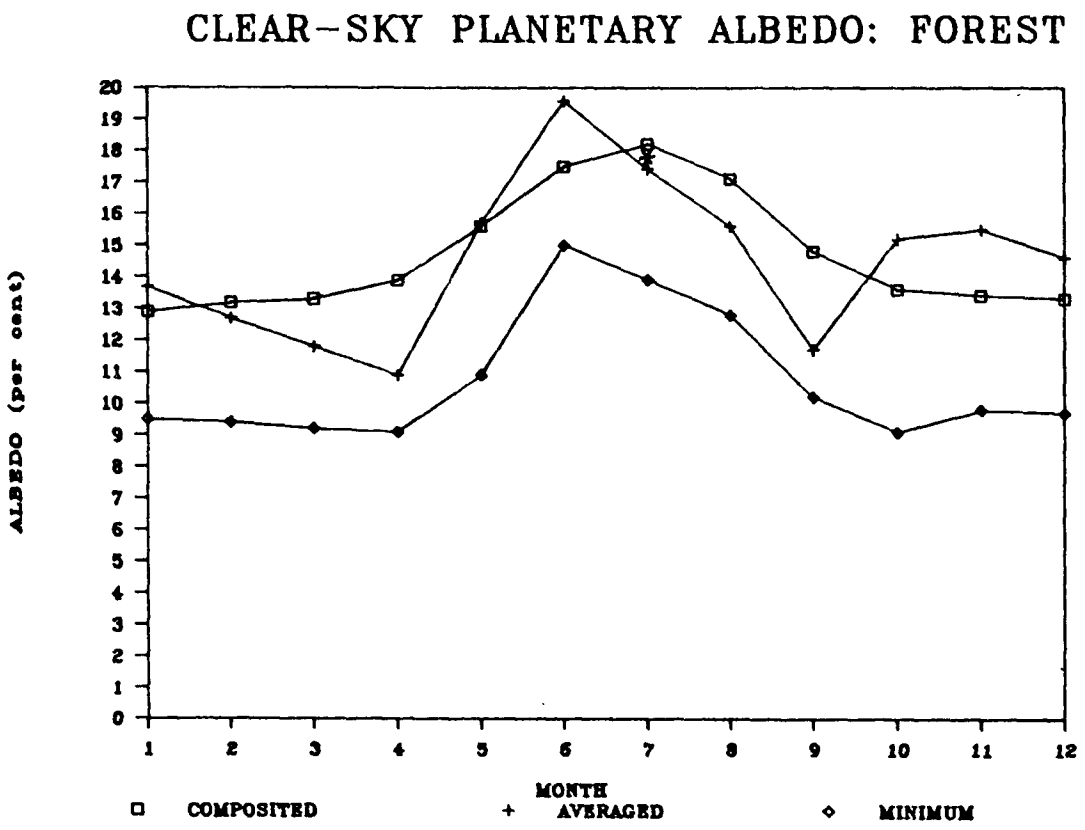

FIG. 10. (*Continued*)

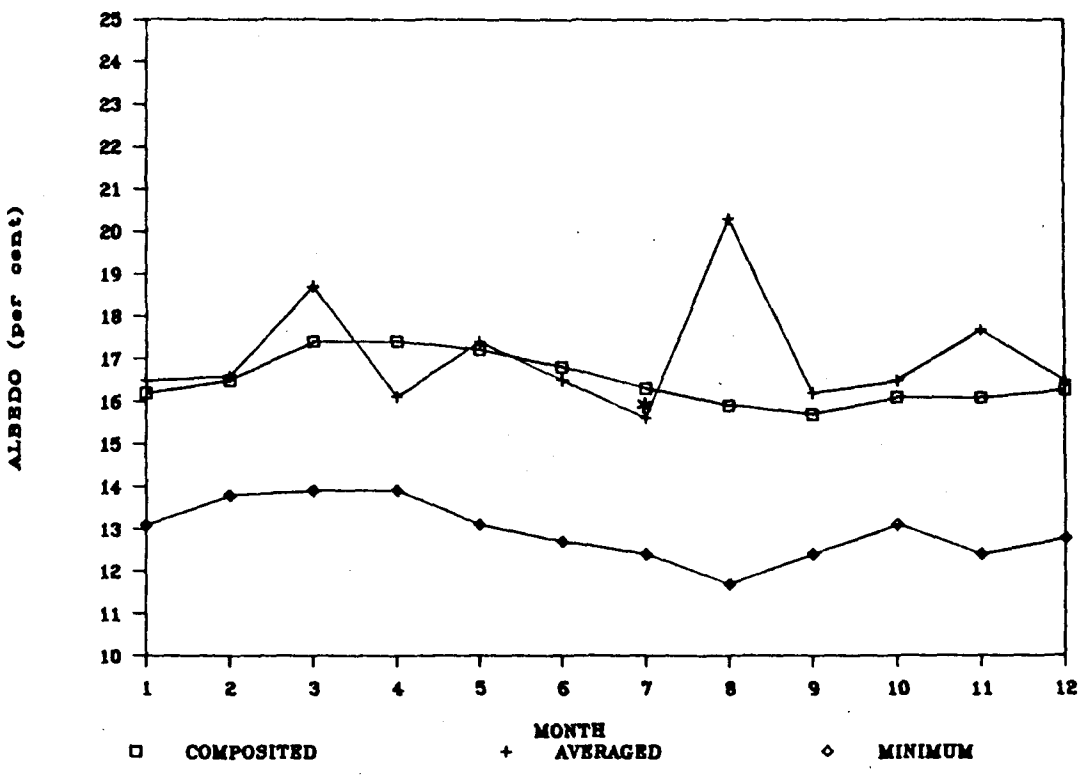

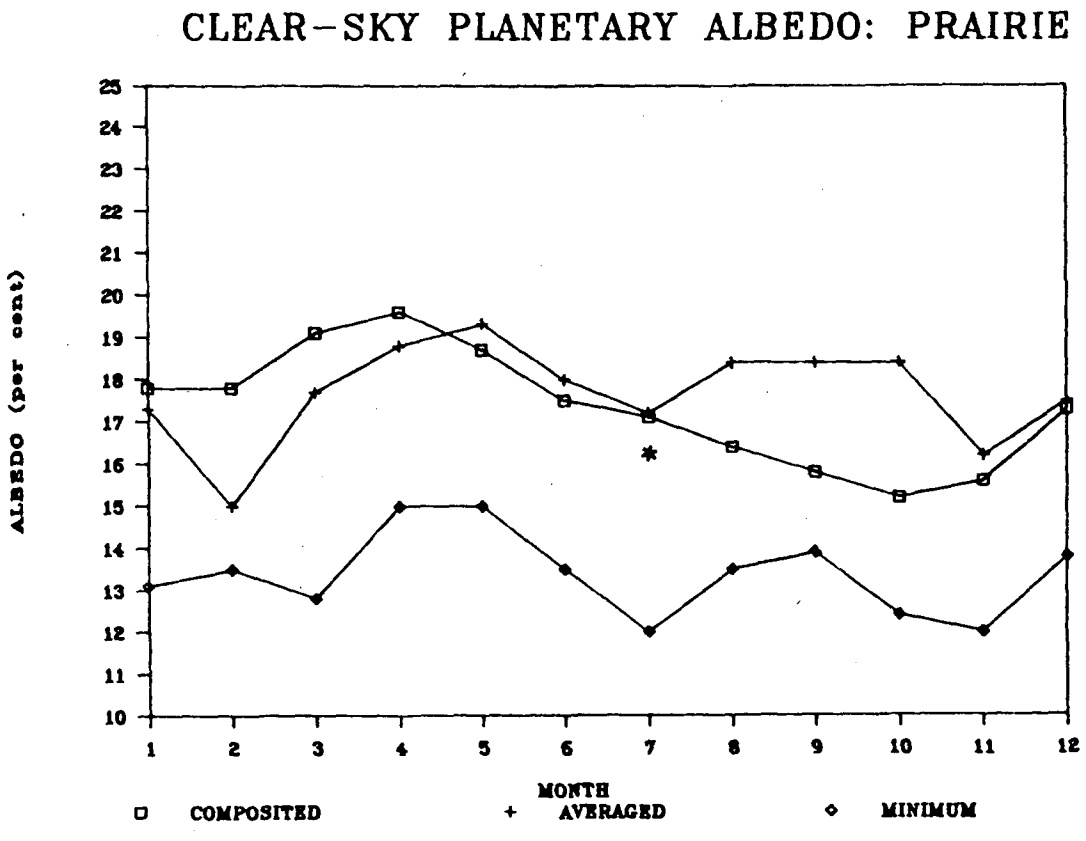

FIG. 11. Same as in Fig. 10 for grass (top) and prairie (bottom).

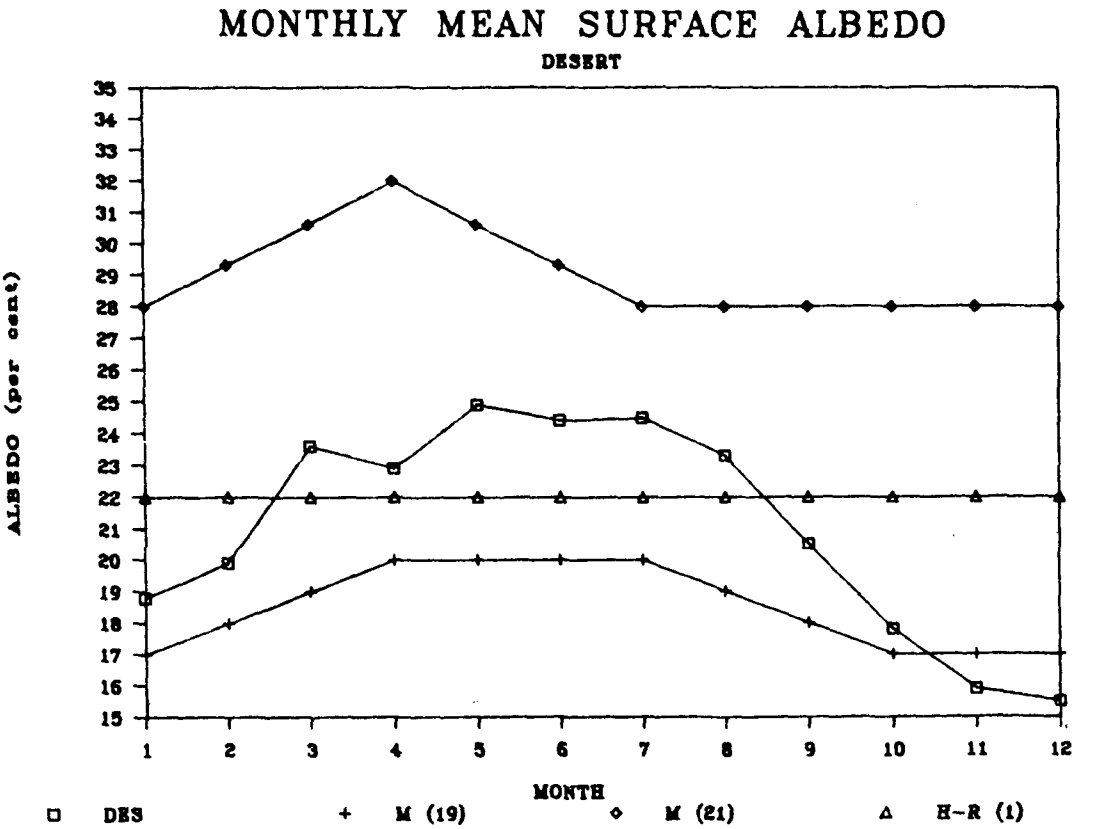

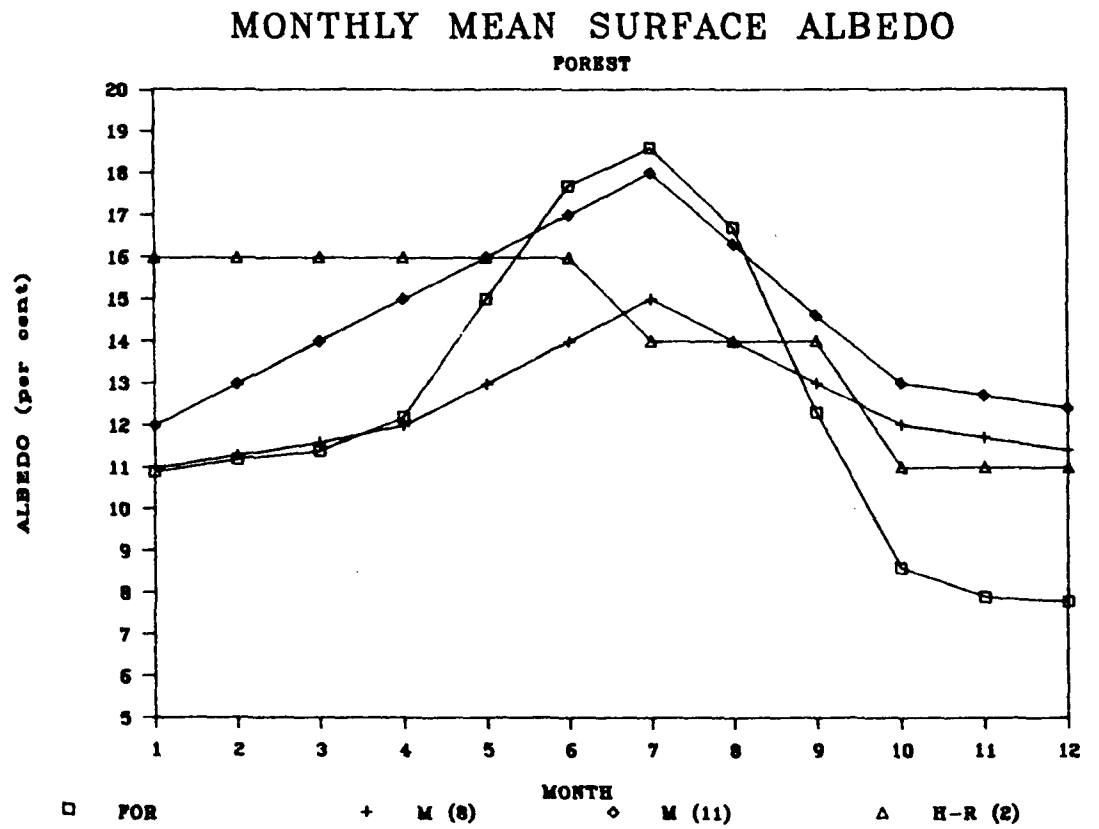

FIG. 12. Annual variation of monthly mean surface albedo obtained by the present method (desert and forest), and albedos reported by Matthews (1985) [vegetation types (19) and (21)] and by Hummel and Reck (1979) [types (1) and (2)], described in the text: desert (top) and forest (bottom).

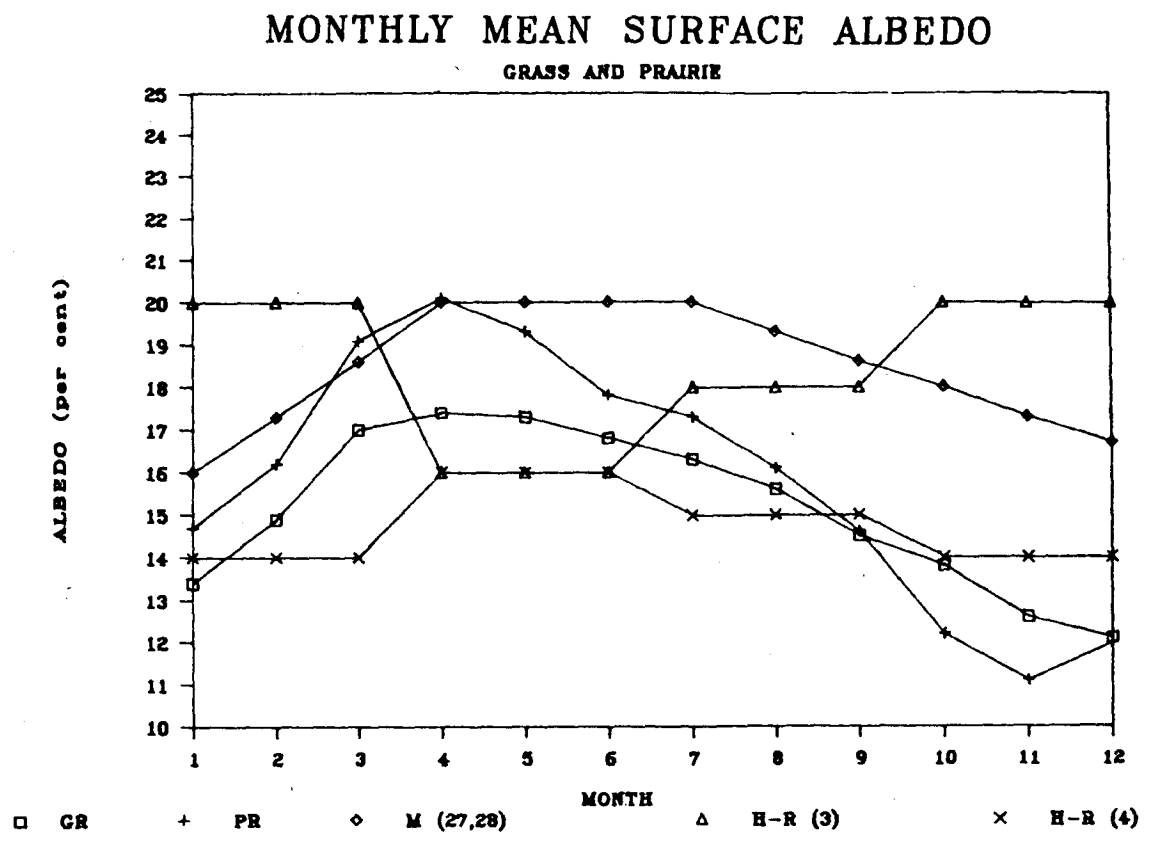

FIG. 13. Same as in Fig. 12 for grass and prairie. Results of the present method (grass and prairie) are compared with albedos from Matthews (1985) [types (27) and (28)] and from Hummel and Reck (1979) [types (3) and (4)], described in the text.

2) Narrow-to-broadband conversion.
3) Cloud-screening.
4) 9-day compositing.
5) Averaging on each day of compositing.
6) Interpolation, filling in missing data.
7) Averaging over the compositing interval.
8) Atmospheric correction.

The proposed method of compositing is based on the established periodicity in observed albedo induced by the systematic variation in sun-target-sensor geometry. In view of the large range of observed albedo variation, it is evident that the "minimum albedo" method may underestimate the monthly mean value. Simple averaging can give a good estimate of the monthly mean albedo only if data are evenly distributed over the geometry combinations. The compositing method enables weighting observations by the number of the corresponding geometry combinations. It is relatively simple and does not require much information. The only input necessary for this method are AVHRR channel 1 and 2 mapped data with the corresponding solar zenith angles. However, even in the absence of information on solar zenith angles, the present approach can be useful as well. Calculations of the monthly mean planetary albedos by taking an arithmetic mean over the interval of compositing showed very small deviations from those obtained by (9). This is due to the fact that the range of variation in the solar zenith angle is relatively narrow for each month. In any event, the result will be closer to the "true" albedo than that obtained by merely taking the minimum value as in the "minimum albedo" method or by a simple averaging of cloud-free data irrespective of the sun-target-sensor geometry. Thus, this method can serve quite well for AVHRR data users who are interested in annual albedo variability but have no other information except for channel 1 and 2 data. As far as cloud screening is concerned, in most cases these data are sufficient. Cloud contamination by a homogeneous layer of transparent (in the shortwave) cirrus cloudiness may not be easily eliminated if thermal data are unavailable. However, the impact of such optically thin clouds on the surface albedo should not be great.

The results of this method depend upon the success of cloud-screening and the number of clear-sky days. Naturally, missing data will introduce errors in the monthly mean estimate. However, due to the monotonic behavior of the composited albedo $\bar{\alpha}$ within the interval of compositing, piecewise linear interpolation should work reasonably well. Future research could be directed towards establishing a universal analytical

function which would contain coefficients dependent upon surface type and season. Then, a Fourier function can be constructed and used for predicting the observed albedo. This of course will require more data to be processed.

The limitations of the present approach include an inability to discriminate between snow and clouds, and the difficulties in cloud detection over areas with high natural spatial variability of albedo. The method of compositing was developed using specifics of scan patterns of the NOAA-9 AVHRR. Therefore, the 9-day cycle may not be valid for another satellite and/or another instrument. The principle, however, should remain appropriate for any cross track scanner onboard polar orbiters. The accuracy of the results is reduced when the scanning deviates further away from the principal plane with increased errors in the case of large solar zenith angles. Therefore, the compositing procedure is most reliable during the growing season in temperate latitudes. Some uncertainty may be associated with the incomplete sampling of the viewing geometry over the hemisphere.

One may argue that the derivation of surface albedo is restricted to an aerosol free atmosphere. However, the error introduced due to the turbidity is small when solar zenith angles are not large and for the range of albedo values of vegetated surfaces (0.1–0.25) under normal conditions (Koepke and Kriebel 1987).

The derivation of surface albedo can be improved by refining both narrow-to-broadband and planetary-to-surface albedo conversions. One should bear in mind, however, that linear correlation techniques may not always be satisfactory because of a possible nonlinearity of combined angular and spectral dependences of atmospheric effects and surface properties (Matthews and Rossow 1987).

In summary, each step of the proposed approach contributes to the overall uncertainty of the final result. When many factors are uncertain, errors are usually analyzed by simulation using measurements as an input to a model (e.g. Koepke and Kriebel 1987). In the present work, we can only roughly estimate the accuracy of the method. Both the narrow-to-broadband conversion and the atmospheric correction have about the same root-mean-square error of 2% albedo units (Wydick et al. 1987; Chen and Ohring 1984). Preliminary results of the comparison of the 9-day compositing and bidirectional model correction suggest that 2% would be a reasonable estimate of the accuracy (Figs. 10 and 11). (Note that all of the above considerations concern the cloud-free data.) One should not forget about the uncertainties inherent to the cloud-screening technique. The derived surface albedos have been tested against some available ground truth. The results of the present method are within the range of uncertainty of the ground based data (Figs. 12 and 13). A better estimate of the accuracy of the present method can possibly be made using data of specially organized experiments.

Despite its limitations, the suggested approach can be employed in producing monthly maps of surface albedos for snow-free land, which makes it useful for climate modeling and monitoring. In particular, it can be applied to the derivation of the radiation budget components at the top of the atmosphere and at the surface of the Earth.

Acknowledgments. Throughout the preparation of this work, discussions with Drs. G. Ohring, D. Tarpley, P. McClain, H. Jacobowitz and G. Rienhardt were very important. The constructive criticism and helpful advice of Drs. A. Gruber and N. Rao are greatly appreciated. Thanks are also due to Dr. I. Ruff for producing the illustration of the NOAA-9 AVHRR scan patterns (Fig. 1) and to Dr. L. Gandin for suggestions during the revision of the manuscript.

REFERENCES

Briegleb, B. P., and V. Ramanathan, 1982: Spectral and diurnal variations in clear sky planetary albedo. *J. Appl. Meteor.*, **21**, 1160–1171.

——, P. Minnis, V. Ramanathan and E. Harrison, 1986: Comparison of regional clear-sky albedos inferred from satellite observations and model computations. *J. Climate Appl. Meteor.*, **25**, 214–226.

Chen, T. S., and G. Ohring, 1984: On the relationship between clear-sky planetary and surface albedos. *J. Atmos. Sci.*, **41**, 156–158.

Dedieu, G., P. Y. Deschamps and Y. H. Kerr, 1987: Satellite estimation of solar irradiance at the surface of the Earth and of the surface albedo using a physical model applied to METEOSAT data. *J. Climate Appl. Meteor.*, **26**, 79–87.

Duggin, M. J., 1985: Factors limiting the discrimination and quantification of terrestrial features using remotely sensed radiance. *Int. J. Remote Sens.*, **6**, 3–27.

Ellis, J. E., and T. H. Vonder Haar, 1978: Solar radiation reaching the ground determined from meteorological satellite data. *Proc. of the Third Conf. on Atmospheric Radiation*, Am. Meteor. Soc., Davis, Ca., June 28–30, 1978.

Gallo, K. P., J. D. Tarpley and D. F. McGinnis Jr., 1986: Land surface climatic variables monitored by NOAA-AVHRR satellites. *Proc. of the ACSM-ASPRS Convention, Vol. 5, remote sensing.* 16–21 March 1986, Washington, D.C., ACSM–ASPRS, Falls Church, Va., pp. 1–8.

Geleyn, J. F., and H. J. Preuss, 1983: Surface albedos derived from satellite data and their impact on forecast models. *Arch. Meteo. Geophys. Bioklim., Series A*, **32**, 353–359.

Gutman, G., 1987: The derivation of vegetation indices from AVHRR data. *Int. J. Rem. Sens.*, **8**, 1235–1242.

——, D. Tarpley and G. Ohring, 1987: Cloud-screening for determination of land surface characteristics in a reduced resolution satellite dataset. *Int. J. Rem. Sens.*, **6**, 859–870.

Gruber, A., G. Gutman, D. J. Tarpley and V. R. Taylor, 1987: Surface albedo estimates from AVHRR data for different land surfaces. Presented at IAMAP/IUGG meeting, Vancouver, Canada, 10–22 August, 1987.

Hummel, J. R., and R. A. Reck, 1979: A global surface albedo model. *J. of Appl. Meteor.*, **18**, 239–253.

Jacobowitz, H., G. Smith and I. Laszlo, 1987: The selection and calibration of narrowband channels for the determination of the Earth's radiation budget. Presented at the North American NOAA Polar Orbiter Users Group meeting, 14–16 July, 1987, Boulder, Colorado.

Koepke, P., and K. T. Kriebel, 1987: Improvements in the shortwave cloud-free radiation budget accuracy. Part I: Numerical study

including surface anisotropy. *J. Climate and Appl. Meteor.*, **26,** 374–395.

Matthews, E., 1985: Atlas of archived vegetation, land-use and seasonal albedo data base. NASA Tech. Memo. 86199, 20 pp.

——, and W. B. Rossow, 1987: Regional and seasonal variations of surface reflectance from satellite observations at 0.6 m. *J. Climate and Appl. Meteor.*, **26,** 170–202.

Minnis, P., and E. F. Harrison, 1984: Diurnal variability of regional cloud and clear-sky parameters derived from GOES data. *J. Climate Appl. Meteor.*, **23,** 993–1051.

Pinker, R. T., 1985: Determination of surface albedo from satellites. *Adv. Space Res.*, **6,** 333–343.

——, and J. A. Razgaitis, 1983: Estimating the solar zenith dependence of the clear-sky planetary albedo for land surfaces from the GOES satellite. *J. of Geophys. Res.*, **C10,** 6007–6011.

——, and J. A. Ewing, 1986: Effect of surface properties on the narrow to broadband spectral relationship in clear sky satellite observations. *Rem. Sens. Env.*, **20,** 267–282.

Pinty, B., and G. Szejwach, 1985: A new technique for inferring surface albedo from satellite observations. *J. Climate Appl. Meteor.*, **24,** 741–750.

Rao, C. R. N., 1987: Prelaunch calibration of channels 1 and 2 of the Advanced Very High Resolution Radiometer. NOAA Tech. Rep., NESDIS 36, U.S. Dept. of Commerce, pp. 66.

Taylor, V. R., and L. L. Stowe, 1984a: Reflectance characteristics of uniform earth and cloud surface derived from Nimbus-7 ERB. *J. Geoph. Res.*, **D4,** 4987–4996.

——, and ——, 1984b: Atlas reflectance patterns for uniform earth and cloud surfaces. NOAA Tech. Rep., NESDIS 10, 66 pp.

Thomasell, A., 1979: Wind analysis by conditional relaxation. NOAA Tech. Rep. NESS 77, U.S. Dept. of Commerce, pp. 23.

Wydick, J. E., P. A. Davis and A. Gruber, 1987: Estimation of broadband planetary albedo from operational narrowband satellite measurements. NOAA Tech. Rep. NESDIS 27, U.S. Dept. of Commerce, pp. 32.